

Coupled dipole method for radiation dynamics in finite photonic crystal structures

Frédéric Bordas,¹ Nicolas Louvion,¹ Ségolène Callard,¹ Patrick C. Chaumet,² and Adel Rahmani¹
¹*Laboratoire d'Electronique, Optoélectronique et Microsystèmes-UMR CNRS 5512-Ecole Centrale de Lyon 36,*
avenue Guy de Collongue, F-69134 Ecully Cedex, France

²*Institut Fresnel (UMR 6133), Université d'Aix-Marseille III, avenue Escadrille Normandie-Niemen,*
F-13397 Marseille cedex 20, France

(Received 24 October 2005; revised manuscript received 3 February 2006; published 2 May 2006)

We present a coupled-dipole treatment of radiation dynamics in the weak-coupling regime in a finite three-dimensional photonic crystal structure. The structure is discretized in real space and the self-consistent local field is computed. We illustrate the computation of radiation dynamics by calculating the spontaneous emission rate for a source located in a defect cavity inside a slab photonic crystal structure. We compute the cavity spectral response, the near-field modal structure, and the far-field radiation pattern of the microcavity. We also discuss our results in light of the recent experimental near-field observations of the optical modes of a photonic crystal microcavity.

DOI: [10.1103/PhysRevE.73.056601](https://doi.org/10.1103/PhysRevE.73.056601)

PACS number(s): 42.70.Qs, 42.25.Fx, 42.25.Bs, 41.20.-q

I. INTRODUCTION

By combining high refractive index contrast and lattice effects, photonic crystals have demonstrated an unprecedented ability to herd and confine photons [1]. Even structures exhibiting an incomplete band gap, which prevent the propagation of photons within a range of frequencies only in some specific directions, have led to an impressive array of new devices. In particular, slablike structures, which rely on total internal reflection for the vertical optical confinement while the photonic band-gap effect controls the in-plane propagation, have become an important brick in the design of new nanophotonic architectures. Passive structures can make, for instance, efficient waveguides and filters [2], while active structures, with embedded sources, can, for instance, make ultralow threshold microlasers [3], or be used as a source of nonclassical light [4]. These structures have also been used to control the dynamics of nanosources and observe inhibition and enhancement of spontaneous emission [5–7].

The ever growing importance of photonic crystals in optics and photonics is matched by the increasing need for numerical methods capable of handling complex configurations. There are a great many numerical methods that can be used to study the electromagnetic properties of a photonic crystal structure. However, when it comes to arbitrary, finite defects in a photonic crystal, two types of approaches are often used. The first one is based on a plane-wave expansion and the use of supercells [8]. The second is the finite difference in time domain (FDTD) technique [9]. In this article, we present a complementary approach based on the coupled dipole method (CDM), which unlike the FDTD operates in the frequency domain and only requires the scatterer to be discretized in real space. Also, in the CDM no explicit boundary conditions need to be specified. Furthermore, because the CDM in its most common formulation deals with finite scatterers, it does not require a supercell formulation (in fact in the CDM it is when dealing with infinite periodic structures that one needs a formulation in terms of elementary cells [10]).

The purpose of this paper is therefore to illustrate how the CDM can be applied to a defect cavity in a finite photonic structure. In particular, we will show how radiation dynamics can emerge naturally from the formulation of the method, and how, once the local fields inside the scatterer are known, the far field can be obtained readily. We will also discuss the field confinement induced by the cavity in light of our recent near-field optics experiments.

We shall consider the weak-coupling regime of the source-cavity system. In this regime, the evolution of the source, assumed to be a two-level system initially in its excited state, is irreversible. The time evolution of the source is characterized by an exponentially decreasing probability to remain in the excited state. The decay rate for this process is given by Fermi's golden rule. We emphasize that within this regime, the normalized decay rate (normalized to a source in an infinite medium) can be calculated classically [11]. This treatment is valid as long as the escape time of the photon out of the cavity is short enough to prevent any memory effect (Markovian regime) in the interaction between the source and the electromagnetic field. Equivalently, this means that the quality factor of the cavity resonance has to be much smaller than the intrinsic quality factor associated with the optical transition of the source. This will clearly be the case for the cavity modes we consider in this paper. Note that for any resonator in general (photonic crystal, microdisk, microsphere,...), the treatment of situations which do not satisfy the approximations we just mentioned requires a more rigorous description of the interaction between the source and the electromagnetic field, including non-Markovian effects [12].

The CDM has been introduced by Purcell and Penny-packer [13] to study the scattering of light by interstellar grains with arbitrary shapes. This method has been used to compute cross sections [14], optical forces [15–17], near-field light scattering [18], and spontaneous emission [19]. The theoretical foundation of the CDM relies on the fact that when an object interacts with an electromagnetic field, it develops a polarization. If one considers a small enough volume inside the object, the induced polarization is uniform

within this volume, and hence that small region can be represented by an electric dipole with the appropriate polarizability. Therefore, any object can be discretized as a collection of dipolar subunits. In this paper, we use the CDM to address the radiation dynamics of a source inside a finite photonic crystal microcavity.

II. COMPUTATION OF THE SELF-CONSISTENT LOCAL FIELD

Consider an arbitrary, three-dimensional object with complex permittivity $\epsilon(\mathbf{r}, \omega)$ [i.e., complex refractive index $n(\mathbf{r}, \omega) = \sqrt{\epsilon(\mathbf{r}, \omega)}$]. When an electromagnetic wave interacts with the object, it creates a linear polarization within the object. The spatial variations of the polarization inside the object depend on the refractive index of the material and the geometry of the object. However, over any small-enough volume inside the object, the polarization can be considered to be uniform and that volume can be represented as an electric dipole. When this principle is applied to the entire scatterer, one obtains the coupled dipole method [13,14]. If we discretize the scatterer over a cubic lattice with period d , we can write the local field at each lattice site as

$$\mathbf{E}(\mathbf{r}_i, \omega) = \mathbf{E}_0(\mathbf{r}_i, \omega) + \sum_{j=1, j \neq i}^N \mathbf{F}_0(\mathbf{r}_i, \mathbf{r}_j, \omega) \alpha(\mathbf{r}_j, \omega) \mathbf{E}(\mathbf{r}_j, \omega), \quad (1)$$

where $\mathbf{E}_0(\mathbf{r}_i, \omega)$ is the incident field, $\mathbf{E}(\mathbf{r}_i, \omega)$ is the local field at position \mathbf{r}_i , and $\alpha(\mathbf{r}_j, \omega)$ is the dynamic polarizability of the volume element located at position \mathbf{r}_j . The tensor $\mathbf{F}_0(\mathbf{r}_i, \mathbf{r}_j, \omega)$ is the free-space linear field susceptibility which gives the field at position \mathbf{r}_i due to a dipole at position \mathbf{r}_j . The case $i=j$ is taken into account in the expression of the polarizability, which can be written as [20]

$$\alpha(\mathbf{r}_j, \omega) = \alpha_0(\mathbf{r}_j, \omega) \times \left[1 - \frac{F_0^{\text{int}}(\mathbf{r}_j, \mathbf{r}_j, \omega) + 4\pi/3}{V_j} \alpha_0(\mathbf{r}_j, \omega) \right]^{-1}, \quad (2)$$

where

$$\alpha_0(\mathbf{r}_j, \omega) = \frac{3d^3}{4\pi} \frac{\epsilon(\mathbf{r}_j, \omega) - 1}{\epsilon(\mathbf{r}_j, \omega) + 2} \quad (3)$$

follows from the Clausius-Mossotti relation. The volume V_j of the j th cell is in our case d^3 . In the present study, the subunit has a cubic shape and ϵ is a scalar; hence the polarizability is a scalar. Then $F_0^{\text{int}}(\mathbf{r}_j, \mathbf{r}_j, \omega)$ is the result of the numerical integration of the component xx of the field-susceptibility tensor \mathbf{F}_0 over the volume of cell j (due to the cubic shape of the subunit, the components yy and zz are equivalent to xx) [20]. However, a simpler, analytical expression of the polarizability can be obtained by integrating the tensor over a spherical region with a volume equal to that of the cubic cell. This yields the expression of the polarizability derived by Lakhtakia [21,22], which simplifies the calculation of the polarizability, without introducing any substantial error compared to the rigorous expression of Eq. (2), as was demonstrated in [20].

The local field at all lattice sites is found by solving the linear system of Eq. (1) iteratively using the quasiminimal residual method of Freund and Nachtigal [23]. The computation of the local field can be accelerated by using the fact that the field-susceptibility tensor actually depends on the relative positions of the source point and the field point, rather than on their absolute locations. This means that $\mathbf{F}_0(\mathbf{r}_i, \mathbf{r}_j, \omega)$ can be written as $\mathbf{F}_0(\mathbf{r}_i - \mathbf{r}_j, \omega)$. This property of the field-susceptibility tensor allows Eq. (1) to be cast as a convolution product which can be computed very efficiently using fast-Fourier transform techniques [24].

Consider a discretization box with dimensions $N_x d, N_y d$, and $N_z d$, which contains the scattering object. We define the polarizability over the box as $\alpha_{i_x, i_y, i_z}(\mathbf{r}_{i_x, i_y, i_z}, \omega) = 0$ for a subunit lying outside the object (note that $i_x = 1, \dots, N_x$, $i_y = 1, \dots, N_y$, and $i_z = 1, \dots, N_z$), and $\alpha_{i_x, i_y, i_z}(\mathbf{r}_{i_x, i_y, i_z}, \omega) = \alpha(\mathbf{r}_j, \omega)$ otherwise. We now double the size of the lattice in each dimension and treat all quantities as periodic in the three dimensions with periods $2N_x$, $2N_y$, and $2N_z$. Note that the actual object is neither doubled in size nor made periodic. This is merely a numerical technique that allows us to treat the convolution product as a cyclic convolution. The matrix containing the field susceptibility is Toeplitz, i.e., each of its elements can be labeled by $i-j$ instead of (i, j) . To use FFTs, we need to embed the Toeplitz matrix into a circulant matrix of twice the size whose element i is equal to element $K-i$ for $0 \leq i \leq K-1$, and where K is the order of the circulant matrix (twice the order of the original matrix). The matrix-vector convolution product can now be computed by FFT after the vector is doubled in size and padded with zeros. The result of the original convolution product is then obtained by cropping the result of the cyclic convolution down to the size of the original vector. Omitting the dependence on ω , we can formally rewrite Eq. (1) as

$$\mathbf{Y}_{i_x, i_y, i_z} = \sum_{j_x=1}^{2N_x} \sum_{j_y=1}^{2N_y} \sum_{j_z=1}^{2N_z} \mathbf{F}_0(\mathbf{r}_{i_x, i_y, i_z} - \mathbf{r}_{j_x, j_y, j_z}) \mathbf{X}_{j_x, j_y, j_z} \quad (4)$$

with $\mathbf{X}_{j_x, j_y, j_z} = \alpha_{j_x, j_y, j_z} \mathbf{E}(\mathbf{r}_{j_x, j_y, j_z})$ for $j_x \leq N_x$ and $j_y \leq N_y$ and $j_z \leq N_z$, and $\mathbf{X} = \mathbf{0}$ everywhere else. It is now obvious that Eq. (4) is a convolution product which can be computed in a very efficient way using a FFT [25].

Once the local field is known at all lattice sites, the scattered field anywhere else can be computed as

$$\mathbf{E}(\mathbf{r}, \omega) = \mathbf{E}_0(\mathbf{r}, \omega) + \sum_{i=1}^N \mathbf{F}_0(\mathbf{r}, \mathbf{r}_i, \omega) \alpha(\mathbf{r}_i, \omega) \mathbf{E}(\mathbf{r}_i, \omega). \quad (5)$$

The scattered field can also be seen as the result of a 2D convolution product by a proper choice of the computation grid. Therefore, the computation of the scattered field can also be accelerated by using FFT techniques. The far-field radiation pattern is readily obtained by taking the asymptotic form of the scattered field [18].

$$\mathbf{E}_{\text{Far}}(\mathbf{r}, \omega) \propto \frac{\omega^2 \exp(i\omega r/c)}{c^2 4\pi r} \left[\sum_{i=1}^N \exp\left(-i\frac{\omega}{c} \mathbf{n} \cdot \mathbf{r}_i\right) \times \alpha(\mathbf{r}_i, \omega) \mathbf{M} \mathbf{E}(\mathbf{r}_i, \omega) \right], \quad (6)$$

where \mathbf{n} is the unit vector \mathbf{r}/r , c is the speed of light in vacuum, and the matrix \mathbf{M} is given by

$$\mathbf{M} = \mathbf{1} - \mathbf{n} \otimes \mathbf{n}. \quad (7)$$

III. COMPUTATION OF THE SOURCE DECAY RATE

The dynamics of a dipole source in the weak-coupling regime can be studied by using the field created by the source and the incident field term \mathbf{E}_0 in Eqs. (1) and (5). Indeed, by computing the work done by the scattered field on the source, one can obtain the spontaneous emission decay rate. Similarly, the dispersive part of the source-field interaction would yield the (classical) frequency shift. It is, however, more compact to compute the self-consistent field susceptibility that accounts for the environment of the source as it allows one to compute at once the decay rate for an arbitrary orientation of the dipole moment of the source.

The principle of the calculation is identical to the derivation of the local field presented in the previous section. Let \mathbf{r}_0 be the position of the source; the self-consistent field susceptibility tensor reads

$$\mathbf{F}(\mathbf{r}_i, \mathbf{r}_0, \omega) = \mathbf{F}_0(\mathbf{r}_i, \mathbf{r}_0, \omega) + \sum_{j=1, j \neq i}^N \mathbf{F}_0(\mathbf{r}_i, \mathbf{r}_j, \omega) \alpha(\mathbf{r}_j, \omega) \mathbf{F}(\mathbf{r}_j, \mathbf{r}_0, \omega). \quad (8)$$

The field susceptibility is therefore computed through the same procedure as the local field in the previous section. The dynamics of the source is derived from the value of the field susceptibility at the source, i.e.,

$$\mathbf{F}(\mathbf{r}_0, \mathbf{r}_0, \omega) = \mathbf{F}_0(\mathbf{r}_0, \mathbf{r}_0, \omega) + \sum_{j=1}^N \mathbf{F}_0(\mathbf{r}_0, \mathbf{r}_j, \omega) \alpha(\mathbf{r}_j, \omega) \mathbf{F}(\mathbf{r}_j, \mathbf{r}_0, \omega). \quad (9)$$

The decay rate and frequency shift, normalized to free-space, for a source with a dipole moment along, for instance, direction x can now be written as [19]

$$\frac{\Gamma_x}{\Gamma_0} = 1 + \frac{3}{2k_0^3} \text{Im}[\mathbf{F}_{xx}(\mathbf{r}_0, \mathbf{r}_0, \omega)], \quad (10)$$

$$\frac{(\Delta\omega)_x}{\Gamma_0} = -\frac{3}{4k_0^3} \text{Re}[\mathbf{F}_{xx}(\mathbf{r}_0, \mathbf{r}_0, \omega)], \quad (11)$$

where $k_0 = \omega/c$. The spontaneous emission rate is proportional to the imaginary part of the field susceptibility (i.e., the local density of states) as it corresponds to the dissipative part of the interaction between the dipole moment of the source and the electromagnetic field. On the other hand, the frequency shift pertains to the dispersive part of the interac-

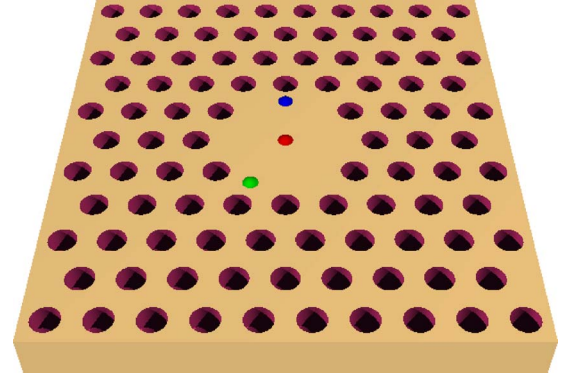


FIG. 1. (Color online) Schematic of the H2 microcavity. The slab thickness is 250 nm. The refractive index is 3.17. The period of the lattice of the photonic crystal is 535 nm. The air hole radius is 178 nm. The source is a dipole located in the middle of the slab. In the figure, we marked the in-plane positions for a dipole at the center, at one corner (left), and at one side (top) of the H2 cavity.

tion and therefore it involves the real part of the field susceptibility at the location of the source. This formulation was compared to the exact analytical result for a source inside a microsphere with excellent agreement [26]. Note that the CDM result includes a local-field factor which can be derived numerically for a substitutional source [26] or calculated analytically for an interstitial source [27]. Here we will use an interstitial source so as to eliminate the local-field effect. We shall also normalize the decay rates to that of a source in the bulk, i.e., an infinite medium with permittivity ϵ .

IV. EXAMPLE

To illustrate the calculation of radiation dynamics inside a finite photonic crystal structure, we consider the configuration of Fig. 1. A slab with dimensions $5350 \times 5125 \times 250 \text{ nm}^3$ and refractive index 3.17 is drilled with air holes (radius 178 nm) on a triangular pattern with period 535 nm. An H2 cavity is created by omitting seven holes.

A source is placed inside the structure at an interstitial position inside the lattice. Vertically the source is located in the middle of the slab. We shall consider several positions of the source inside the cavity. We discretize the structure with a lattice size $d=25 \text{ nm}$ and use Eqs. (8)–(10) to compute the decay rate normalized to free space. We further normalize the results to the decay rate of a source in an infinite medium of permittivity ϵ (which is $\sqrt{\epsilon}$ times the free-space decay rate). Note that this implies that we factor out the local-field effect which can be done readily as the local-field factor can be derived analytically for any arbitrary interstitial position of the source in the lattice [27].

By changing the radiation wavelength of the source, we can also probe the optical modes of the cavity. Figure 2 shows the spontaneous emission rate spectra for a source placed at three locations inside the cavity: at the center, near a corner, and at one side of the cavity. The orientation of the dipole moment of the source is given in the inset. We observe several resonances separated by regions where the de-

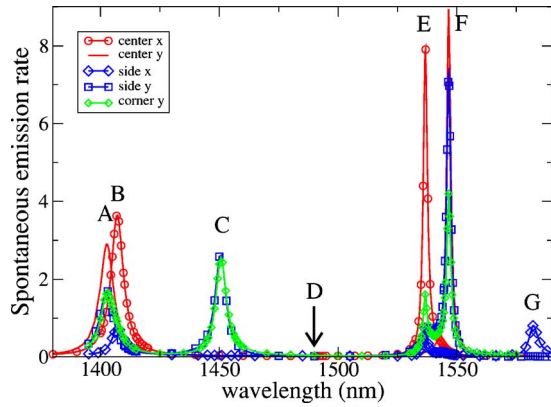


FIG. 2. (Color online) Decay rate, normalized to a source in bulk for a dipole located at the three positions marked in Fig. 1. The position and orientation of the dipole are given in the inset.

decay rate is almost zero. These regions are the illustration of the effect of the photonic band gap on the radiation dynamics of the source. Photon emission by the source is inhibited in those electromagnetic modes that are forbidden by the photonic crystal. Although this is not a three-dimensional photo-

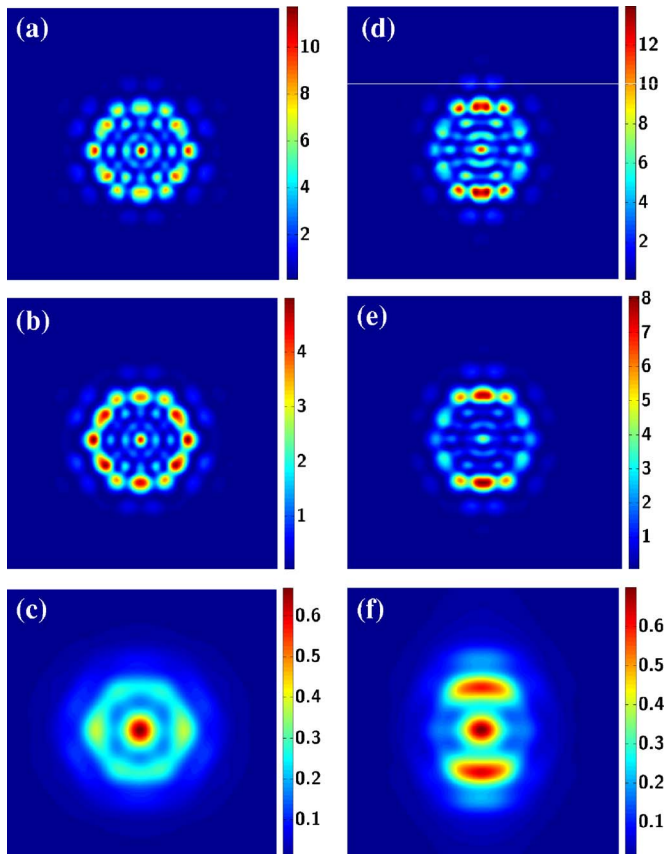


FIG. 3. (Color online) Square of the modulus of the electric field (arbitrary units) above the cavity at the wavelength of modes labeled A (left column) and B (right column) in Fig. 2. The result has been averaged over all orientations of the dipole moment of the source in an xy plane. The maps are computed at different heights z above the cavity. (a) and (d) $z=50$ nm; (b) and (e) $z=100$ nm; (c) and (f) $z=500$ nm.

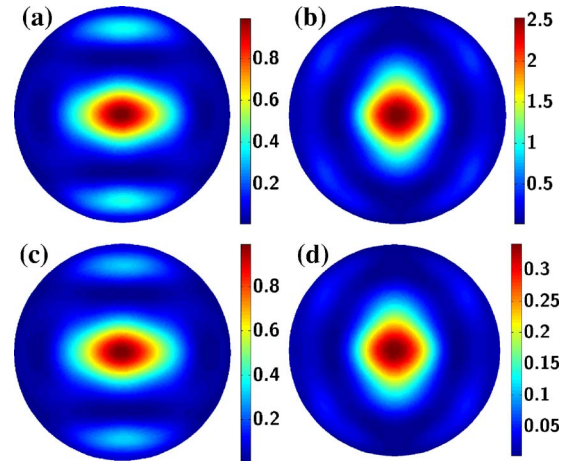


FIG. 4. (Color online) Far-field intensity radiation pattern in the half-space above the cavity for modes labeled A [top row, i.e. (a) and (b)] and B [bottom row, i.e., (c) and (d)] in Fig. 2. Left column [(a) and (c)]: the source is a dipole oriented along x . Right column [(b) and (d)]: the source is a dipole oriented along y . The intensities are normalized to the maximum intensity for a dipole oriented along the x direction.

nic crystal, one can see that the combination of photonic band-gap effect by the periodic array of holes, and refractive confinement (total internal reflection) by the slab, leads to a quite effective inhibition of spontaneous emission at some frequencies. On the other hand, the resonances that we observe correspond to an enhancement of the spontaneous emission of the source by the modes of the cavity. We can also note that for a given frequency of emission of the source, the spontaneous emission rate depends on the location and the orientation of the dipole moment of the source. This reflects the fact that in order to obtain a good electromagnetic coupling between the source and the cavity, the source needs not only to overlap spectrally with the cavity modes (where the density of states is larger), but also spatially, since the coupling term involves the product of the dipole moment of the source with the electric local field at its location; i.e., the dynamics of the source depends on the *local* density of states [28,29].

We have illustrated how the electromagnetic response of the cavity and the radiation dynamics of the source can be computed simultaneously. We now turn our attention to the spatial distribution of light in the near-field of the cavity. Near-field intensity maps can be computed using Eq. (5). We emphasize that because the CDM only requires that the scatterer be discretized, the computation of the scattered field is not restricted to lattice sites. Note that the field maps can be computed efficiently as cyclic convolution products as described previously for the computation of the local field. We plot in Fig. 3 the square of the electric field at a distance z above the cavity. The left column corresponds to the cavity mode labeled A in Fig. 2, whereas the right column pertains to mode B. In an ideal structure, modes A and B are degenerate. In our case, the degeneracy is lifted by our discretization of the cavity. The two modes, however, retain a similar pattern, with a prevailing direction given by x (dipole along y) for mode A and y (dipole along x) for mode B. What is

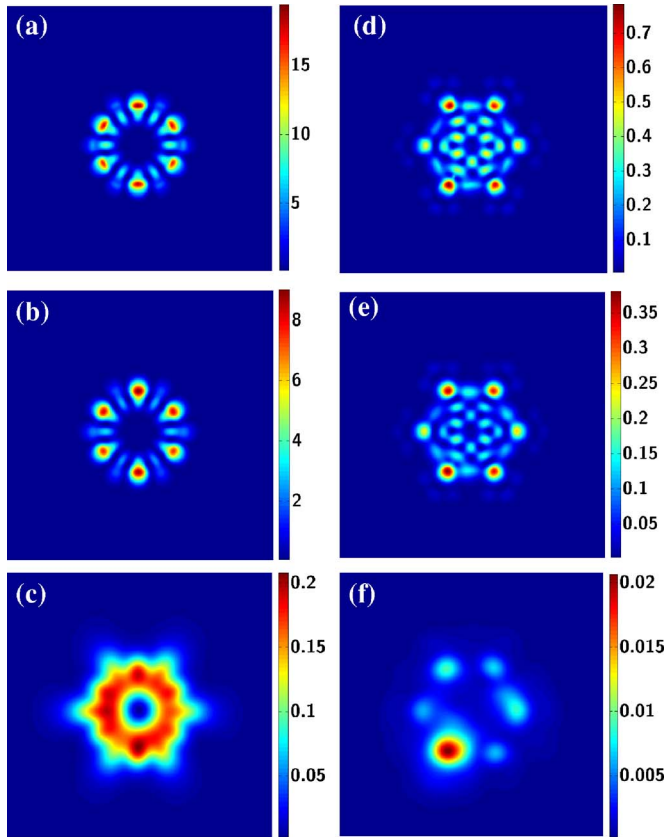


FIG. 5. (Color online) Square of the modulus of the electric field (arbitrary units) above the cavity at the wavelength of modes labeled C (left column) and D (right column) in Fig. 2. The result has been averaged over all orientations of the dipole moment of the source in an xy plane. The maps are computed at different heights z above the cavity. (a) and (d) $z=50$ nm; (b) and (e) $z=100$ nm; (c) and (f) $z=500$ nm.

also interesting is that the finer details of the mode structure wash out quite quickly as one moves away from the surface of the cavity. Figures 3(c) and 3(f), for instance, are computed 500 nm above the cavity and do not show any of the detail still visible at 100 nm [Figs. 3(b) and 3(e)]. This low-pass filtering of high spatial modes is another reason for using near-field techniques to observe the mode pattern of this type of structure [30].

As we mentioned in Sec. II, the far-field radiation pattern can be computed easily once the local field is known in the scatterer. In Fig. 4, we plot the intensity radiation pattern of the two modes. The patterns are normalized to the maximum intensity for a source transition moment oriented along x . Figures 4(a) and 4(b) pertain to mode A, whereas Figs. 4(c) and 4(d) pertain to mode B. These far-field patterns are in agreement with the spectrum, namely they show that modes A and B correspond to an y and x dipole, respectively. Furthermore, the obvious similarities between the far-field patterns of the two modes illustrate that these two modes are in fact degenerate and that although the discretization removes the degeneracy, it does not induce any significant perturbation on the far-field radiation patterns of the two modes. Note that experimentally the mode degeneracy is usually lifted

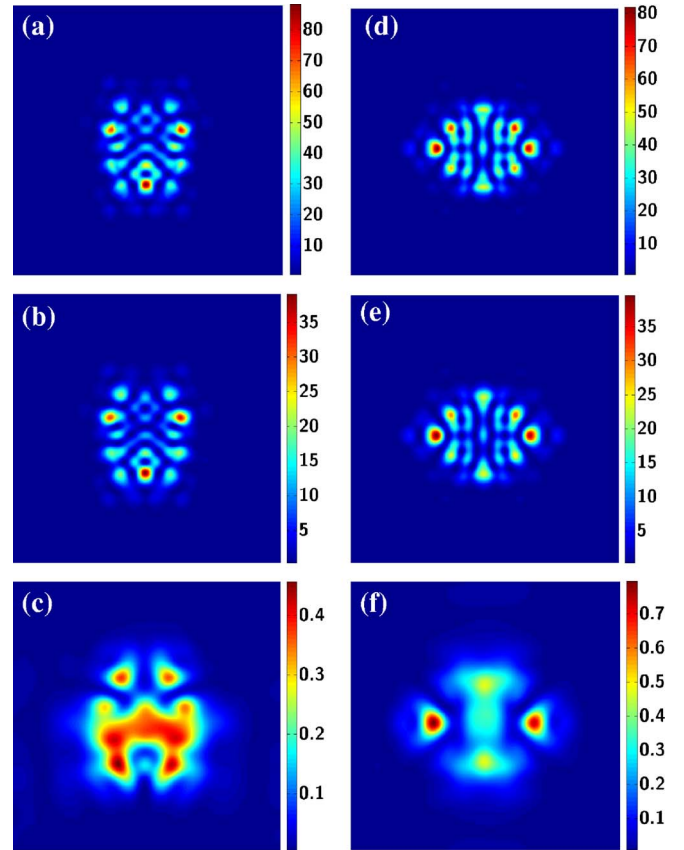


FIG. 6. (Color online) Square of the modulus of the electric field (arbitrary units) above the cavity at the wavelength of modes labeled E (left column) and F (right column) in Fig. 2. The result has been averaged over all orientations of the dipole moment of the source in an xy plane. The maps are computed at different heights z above the cavity. (a) and (d) $z=50$ nm; (b) and (e) $z=100$ nm; (c) and (f) $z=500$ nm.

because of the structural fluctuation of the crystal parameters and the finite size of the structure.

The elusive nature of the evanescent components of the optical modes is emphasized further in the behavior of the mode labeled C [Figs. 5(a)–5(c)]. This mode exhibits a pattern of six spots located at the center of the six walls (sides) of the cavity. However, only 500 nm above the cavity, the structure of the mode has disappeared to leave a ring-shaped field pattern. Note that this evolution with the distance to the cavity has recently been observed with a near-field scanning optical microscope [30]. Again, this illustrates the need to be within the near field of the cavity to observe the actual mode structure.

The field map shown in Figs. 5(d), 5(e), and 5(f) is different from the other ones in that it corresponds to a very weak resonance labeled D on the spectrum (not visible on the scale of Fig. 2). What is interesting about this field map is that such a mode with bright spots at the six corners of the cavity has been observed experimentally using a scanning near-field optical microscope; this mode appeared as a peak in the near-field spectrum, whereas it was absent from the far-field spectrum [30]. Our calculation allows us to gain some insight into the nature of this mode. The field intensity

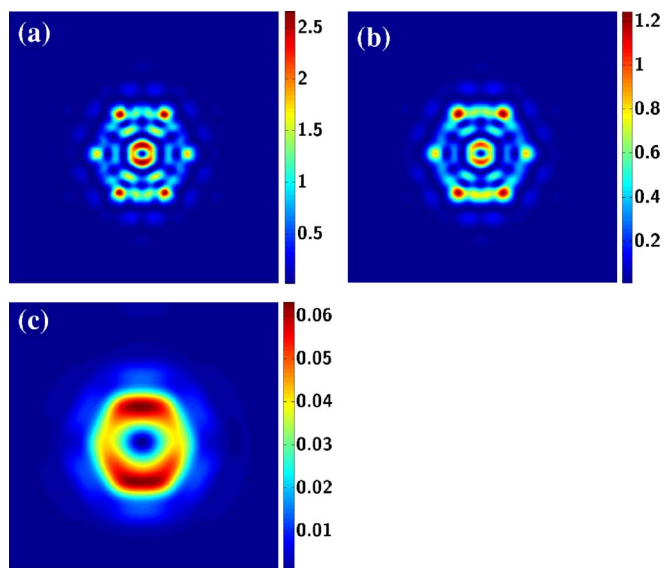


FIG. 7. (Color online) Square of the modulus of the electric field (arbitrary units) above the cavity at the wavelength of the mode labeled G in Fig. 2. The result has been averaged over all orientations of the dipole moment of the source in an xy plane. The maps are computed at different heights z above the cavity. (a) $z=50$ nm; (b) $z=100$ nm; (c) $z=500$ nm.

map computed 500 nm above the cavity [Fig. 5(f)] shows that the main contribution to the intensity comes from the source (located in the lower left corner of the cavity) rather than from the optical mode inside the cavity. This shows that we are dealing with a very weak resonance of the cavity.

Similar field map calculations for the modes labeled E through G on the spectrum are shown in Figs. 6 and 7. Although the modeling of the interaction of the near-field probe with the optical mode of the cavity is beyond the scope of

this paper, we can make a few comments. Modes E and F are twofold degenerate, which makes it difficult to observe a clear pattern in the near field as confirmed by experiments [30]. On the other hand, we note that the experimental near-field map of mode G is in good agreement with the observed pattern if we consider the map computed 500 nm above the cavity. This is most likely due to the finite size of the optical probe in the experiment, which leads to a low-pass filtering of the field pattern. In an actual experiment also, because of the vertical extension of the probe the interaction occurs over a finite region above the cavity, not a single plane, which, depending on the mode pattern, can lead to an intensity map that differs from the one computed without accounting for the probe.

V. CONCLUSION

We have presented a coupled dipole treatment of the problem of a source embedded in a cavity inside a finite photonic crystal structure. We have illustrated the approach on an H2 photonic crystal microcavity for which we computed the cavity spectrum, the Purcell effect, the near-field map, and the far-field radiation pattern. We also discussed our results in light of the recent near-field optical probing of an H2 and found excellent agreement with the experimental results. We have thus demonstrated that the CDM can be used to address radiation dynamics in an arbitrary, finite photonic crystal structure.

ACKNOWLEDGMENTS

This work is supported by the Ministère délégué à la Recherche et aux Nouvelles Technologies through an “ACI Jeune Chercheur” Grant.

-
- [1] E. Yablonovitch, *Phys. Rev. Lett.* **58**, 2059 (1987).
 - [2] E. Drouard, H. T. Hattori, C. Grillet, A. Kazmierczak, X. Letartre, P. Rojo-Romeo, and P. Viktorovitch, *Opt. Express* **13**, 3037 (2005).
 - [3] J. Mouette, C. Seassal, X. Letartre, P. Rojo-Romeo, J. L. Leclercq, P. Regreny, P. Viktorovitch, E. Jalaguier, P. Perreau, and H. Moriceau, *Electron. Lett.* **39**, 526 (2003).
 - [4] J. Vuckovic, D. Englund, D. Fattal, E. Waks, and Y. Yamamoto, *Physica E (Amsterdam)* **31**, 2 (2006).
 - [5] M. Fujita, S. Takahashi, Y. Tanaka, T. Asano, and S. Noda, *Science* **308**, 1296 (2005).
 - [6] D. Englund, D. Fattal, E. Waks, G. Solomon, B. Zhang, T. Nakaoka, Y. Arakawa, Y. Yamamoto, and J. Vuckovic, *Phys. Rev. Lett.* **95**, 013904 (2005).
 - [7] K. Kounoike, M. Yamaguchi, M. Fujita, T. Asano, J. Nakanishi, and S. Noda, *Electron. Lett.* **41**, 1402 (2005).
 - [8] S. G. Johnson and J. D. Joannopoulos, *Opt. Express* **8**, 173 (2001).
 - [9] A. Taflov and S. C. Hagness, *Computational Electrodynamics: The Finite-Difference Time-Domain Method*, 2nd ed. (Artech House, Norwood, MA, 2000).
 - [10] P. C. Chaumet, A. Rahmani, and G. W. Bryant, *Phys. Rev. B* **67**, 165404 (2003).
 - [11] S. Haroche, in *Fundamental Systems in Quantum Optics*, edited by J. Dalibard, J. M. Raimond, and J. Zinn-Justin (North-Holland, Amsterdam, 1992), pp. 767–940.
 - [12] B. Fain, *Phys. Rev. A* **37**, 546 (1988).
 - [13] E. M. Purcell and C. R. Pennypacker, *Astrophys. J.* **186**, 705 (1973).
 - [14] B. T. Draine, *Astrophys. J.* **333**, 848 (1988).
 - [15] B. T. Draine and J. C. Weingartner, *Astrophys. J.* **470**, 551 (1996).
 - [16] P. C. Chaumet and M. Nieto-Vesperinas, *Phys. Rev. B* **61**, 14119 (2000); **62**, 11185 (2000); **64**, 035422 (2001).
 - [17] P. C. Chaumet, A. Rahmani, and M. Nieto-Vesperinas, *Phys. Rev. Lett.* **88**, 123601 (2002).
 - [18] A. Liu, A. Rahmani, G. W. Bryant, L. Richter, and S. Stranick, *J. Opt. Soc. Am. A* **18**, 704 (2001).
 - [19] A. Rahmani, P. C. Chaumet, and F. de Fornel, *Phys. Rev. A* **63**, 023819 (2001).

- [20] P. C. Chaumet, A. Sentenac, and A. Rahmani, *Phys. Rev. E* **70**, 036606 (2004).
- [21] A. Lakhtakia, *Int. J. Mod. Phys. C* **3**, 583 (1992).
- [22] A. Lakhtakia and G. Mulholland, *J. Res. Natl. Inst. Stand. Technol.* **98**, 699 (1993).
- [23] R. W. Freund and N. M. Nachtigal, *Numer. Math.* **60**, 315 (1991).
- [24] J. J. Goodman, B. T. Draine, and P. J. Flatau, *Opt. Lett.* **16**, 1198 (2001).
- [25] We use the FFT code of D. Takahashi (<http://www.ffte.jp/>).
- [26] A. Rahmani and G. W. Bryant, *Phys. Rev. A* **65**, 033817 (2002).
- [27] A. Rahmani, P. C. Chaumet, and G. W. Bryant, *Opt. Lett.* **27**, 430 (2002).
- [28] R. Sprik, B. A. van Tiggelen, and A. Lagendijk, *Europhys. Lett.* **35**, 256 (1996).
- [29] R. C. McPhedran, L. C. Botten, J. McOrist, A. A. Asatryan, C. M. de Sterke, and N. A. Nicorovici, *Phys. Rev. E* **69**, 016609 (2004).
- [30] N. Louvion, D. Gérard, J. Mouette, F. de Fornel, C. Seassal, X. Letartre, A. Rahmani, and S. Callard, *Phys. Rev. Lett.* **94**, 113907 (2005).